MECHANISMS AND MECHANICS OF DEBOND FRACTURES ALONG METAL MATRIX COMPOSITE INTERFACES

A.S. Argon and M.L. Seleznev
Massachusetts Institute of Technology
Cambridge, MA 02139, USA
C.F. Shih and X.H. Liu
Brown University
Providence, R.I. 02912, USA

ABSTRACT

In metal matrix composites toughness is derived primarily from the plastic work of rupture of ductile matrix ligaments between the fractured fibers. Optimization of tensile strength in the longitudinal and transverse directions together with the respective works of fracture requires control of the extent of debonding between the fibers and the matrix which develops in the course of deformation in a continuously changing mix of modes. In Al_2O_3 fiber reinforced Al alloy matrix composites an effective means of controlling the key interface fracture toughness is through coarsening of intermetallic interface precipitates which prescribe a ductile fracture separation layer. A combined experimental approach and micromechanical modeling, utilizing a specially tailored novel tension/shear, traction/separation law provides the means for further optimization of overall behavior.

INTRODUCTION

While metal matrix composites offer remarkable potential for applications in load bearing structural elements at intermediate to high homologous temperatures, short of long term creep conditions, in the metal matrix, barring a few outstanding examples such as diesel engine piston heads, this potential has not been fully realized. This is because the development of these composites has largely been fragmented into pre-conceived areas of importance such as processing, fiber development, matrix/fiber compatibility, and a limited set of performance controlling factors, and the like, rather than considering the major factors and their interactions that govern composite performance. Particularly in the area of achieving combined high axial and transverse strength and high work of fracture, very substantial improvements are possible through a newly developed process of interface structure control. This process is based on placement of a pedigreed population of intermetallic compound precipitates on the fiber/matrix interface that provide a wide range of control of the traction separation relationship, and thereby achieves desired levels of interface debonding that governs matrix ligament rupture and resistance to axial shearing off.

Here we present the details of this finding and the means of analysis of composite behavior

through a specific micromechanics model specially developed for this purpose.

MECHANISMS AND MECHANICS OF FRACTURE IN COMPOSITES

Basic Strategies and Mechanisms

In ceramic matrix composites consisting of strong fibers and brittle matrixes fiber pull-out during the final stages of fracture often provides the only means of affecting the work of fracture. To nurture this in continuous fiber composites, a certain variability of fiber strength is needed to arrange for a degree of randomness of primary fractures in the fibers by balancing the tendency of planar fracture cascades arising from strong mechanical coupling of fiber fractures against variability in fiber strength. While this accomplishes the desired goal of producing non-planar primary fractures and a range of broken fiber engagement lengths ready for pull-out, a substantial potential for composite strength is compromised by the required variability in strength (Argon, 1974). When aligned discontinuous fibers are used the length of these fibers is chosen to maximize the full out work while just preventing additional fiber fractures - all again at the expense of the ultimate strength of the composite.

In metal matrix composites with strong fibers and ductile matrixes, under ideal conditions this compromise is not necessary because the post-fiber fracture work is not derived from fiber pull out but rather from the plastic work of fracture of the metal matrix. Thus, fibers of higher strength and lower variability can be used resulting in composites of higher axial strength. While this produces planar fracture cascades in parallel fibers with little energy absorption, substantial overall fracture work is supplied by the work of rupture of the remaining metal ligaments, as shown in the micrograph of Fig. 1 of a transverse section of a fractured metal matrix composite that is the subject of the presentation which follows.

The sketches of Fig. 1a show two components of the axial fracture process in a continuous fiber metal matrix composite. Primary fiber fracture cascades initiated at different levels produce planar fractures which we label as Mode A. In these the dissipative processes affecting fracture work are the ligament ruptures in the metal matrix over a debonding length L_D. The primary Mode A fractures are bridged by Mode B type simple shear fractures. In the fracture of strong composites the fraction of Mode B fracture is generally small in comparison with the Mode A fracture. Therefore, in what follows we consider only the Mode A type separations. However, the methodology that will be presented is equally capable of dealing with the Mode B contribution to the overall fracture work.

An elementary analysis of the Mode A fracture work, ignoring all other aspects except the rupture of the metal matrix ligaments as depicted in Fig. 1a, results in a simple expression for the specific fracture work X_A of,

$$X_A = \frac{1}{\sqrt{3}}(1 - \nu_f)\sigma_o L_D, \tag{1}$$

where ν_f is the volume fraction of fibers, σ_o the matrix tensile plastic resistance in a non-hardening model, and L_D is the debonding length (Friler et al, 1993). Clearly, this debond length is an important element in this fracture process. Very tough interfaces result in

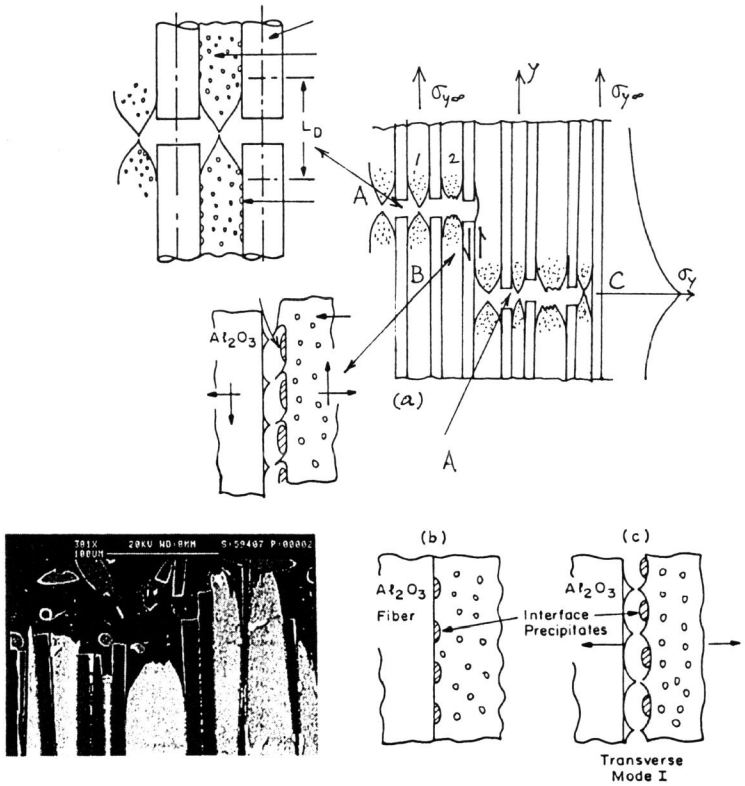

Fig. 1. Forms of interface fracture in a metal matrix composite: a) Modes A of tensile, and B, of shear fracture in a composite, with insets depicting the mixed mode of interface debonding fractures ocurring in Modes A and B; b) depiction of interface fracture of the composite, in the transverse direction.

negligible debonding and in very low energy absorption in the axial fracture of the composite, while excessive debonding beyond the natural necking length adversely affects the transverse strength of the composite. The actual development of debonding in response to a deformation-governed mix of modes of interface fracture is the subject of the micromechanical model. In the particular metal matrix systems composed of sol-gel derived Al_2O_3 polycrystalline fibers and aluminum alloy matrixes fracture in the particular mix of modes is

governed by the interface precipitates, their volume fraction and actual size. The separation toughness by an arbitrary mix of modes is controlled by Al_2Cu precipitates, the control of which is the basis of the present approach in governing overall properties of the composite.

The Composite

The specific metal matrix system of interest is made up of sol-gel derived polycrystalline Al_20_3 (Nextel 610) fibers of 10μm diameter with an average strength of 1.78 GPa and a variance of 0.18 in strength (Weibull exponent of 4.6) occupying a volume fraction of $\nu_f = 0.5$. The Al casting alloy matrix (Type 224) is composed of 5.15% Cu, 0.12% Fe, and 0.34% Mn in which the principal intermetallic precipitate is Al_2Cu. The tensile yield strength of the as cast alloy is 330 MPa, reaching 530 MPa at peak aging. When overaged, the flow stress is roughly 250 MPa.

Of primary interest are the coarsening kinetics of the precipitate particles and their states of adhesion to the fibers and the matrix. The equilibrium volume fraction of particles in the matrix is close to 0.2. The precipitates in the volume have shapes ranging from equiaxed to lenticular, with extreme aspect ratios of around 5. The precipitates on the fiber/matrix interfaces have roughly the same area fraction of coverage with similar ranges of aspect ratio. The coarsening of the precipitates on the interfaces obeys a $t^{\frac{1}{4}}$ law, indicating interface diffusion control. Over the range of time observed (100 hrs) at 350-400C the average particle size increases from 0.4μm to about 1.0μm. Contact angle measurements lead to estimates of works of adhesion (decohesion) between the particles and Al_20_3 fibers and Al matrix of 0.3J/m^2 and 0.85J/m^2 respectively. Parenthetically, it is well known that Al_20_3 (the self oxide) adheres to Al tenaciously.

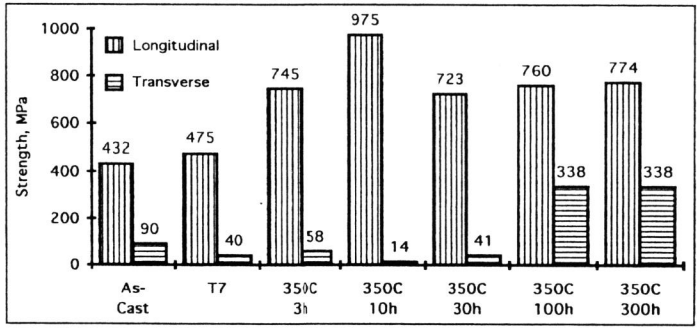

Fig. 2. Responses of longitudinal (axial) and transverse tensile strengths to aging time producing precipitate coarsening in the Nextel 610/Al-224 composite.

Phenomenology of Composite Fracture

The results of fracture experiments on initially intact (free of macrocracks) composites in the axial and transverse direction are summarized in Fig. 2. The figure shows that with aging at 350C the composite tensile strength increases monotonically by more than a factor of 2 and reaches a level of 975 MPa at peak aging of the composite in about 10 hrs. This is qualitatively what should be expected from a rule of mixtures response of the composite due to the systematic increase of the plastic resistance of the matrix. For longer periods of aging the strength decreases and levels off at roughly 750 MPa as the matrix overages. Meanwhile the transverse strength of the composite remains roughly flat at about 40 MPa over aging times up to 30 hrs, but increases sharply to a level of 338 MPa after 100hrs. The dramatic rise of transverse strength at about 50hrs of aging coincides roughly with the full coarsening of the interface precipitates. This must indicate, at least in part, an increase of the resistance to crack growth parallel to the fiber/matrix interfaces, where the increased resistance is derived from the well known increase of fracture toughness with increase in the microstructural scale. A more quantitative evaluation of these results discussed below will indicate that additional effects must also be at play.

Fracture Along Fiber Matrix Interfaces

Detailed examinations of the fracture surfaces of the composites have verified the mechanisms of separation sketched out in Fig. 1. These examinations showed that in the interface

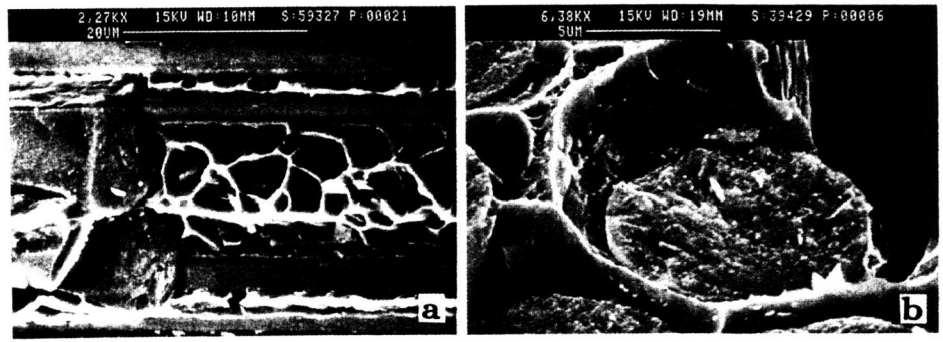

Fig. 3. a) Transverse fracture surface showing fracture surface dimples on the matrix side showing precipitate particles continue to adhere to the Al matrix, b) fully developed rupture in remaining metal ligament, following fiber fracture.

debonding under a deformation induced mix of modes I and II, prior to the matrix ligament ruptures, debonding occurs preferentially between the Al_2Cu precipitates and the Al_20_3 fibers which has the lowest work of adhesion. The particles remain well adhered to the Al matrix which itself remains well adhered to the Al_20_3 fibers. The separation at the interface then occurs by a series of ductile dimple ruptures in a combination of normal separation and shear modes depicted in the lower left inset of Fig. 1a. Transverse composite fracture similarly occurs, by a direct mode I type separation by ductile dimple ruptures as depicted in Fig. 1b. Figures 3a and 3b show direct evidence for this form of separation (Seleznev et al, 1993).

Clearly, the key of the fiber matrix debonding process, establishing the length L_D resides in the effective traction separation characteristic of the matrix at the interface by ductile cavitation under the local mix of mode I and II. A model of this behavior is discussed in the following section.

Micromechanics Model of Mode A Fractures

Methodology

To develop a better understanding of Mode A fractures a micromechanical model was developed which has built on previous methodology developed by Suo and Shih (1993) and Varias et al (1990). In the Mode A type planar separation of the composite the fundamental unit cell problem to be solved is depicted in Fig. 4 for a typical 0.5/0.5 fraction of fiber and matrix - being considered as a plane strain problem. The Al_20_3 sheet (fiber) is taken as initially cracked and responding only elastically, while the constitutive law for the metal matrix is taken as elastic-plastic-power-law hardening, which in uniaxial tension is:

$$\frac{\epsilon^e}{\epsilon_o} = \frac{\sigma}{\sigma_o} \qquad \frac{\epsilon^p}{\epsilon_o} = \left(\frac{\sigma}{\sigma_o}\right)^{1/N} - 1 \quad (\sigma \geq \sigma_o) \tag{2a, b}$$

where σ_o is the yield strength, $\epsilon_o = \sigma_o/E, 1/N$ is the hardening exponent, and E is the Young's modulus. The plasticity is taken to follow the J_2 flow rule. A very important element of the fiber/matrix interaction is the tension/shear, traction-separation (t-s) law associated with the ductile cavitation of the interface, starting with the decohesion of the interface precipitates, from the fiber, discussed above and depicted in Fig. 1. In the absence of more specific experimental information, the (t-s) response was taken to result from a traction potential. Thus,

$$\Phi(\delta_n, \delta_t) = \delta_n^c \int_o^\lambda \sigma(\lambda)' d\lambda' \tag{3}$$

which defines the normal, T_n, and tangential, T_t, components of the tractions offered by the separating interface given by (Tvergaard and Hutchinson, 1993)

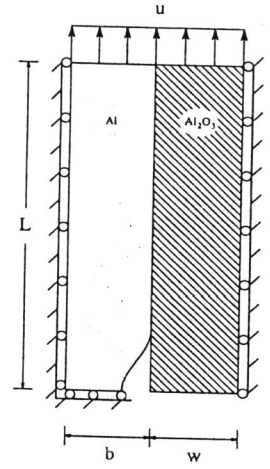

Fig. 4. Computational cell for longitudinal tension in a plane strain idealization.

$$T_n = \frac{\partial \Phi}{\partial \delta_n} = \frac{\sigma(\lambda)}{\lambda}\frac{\delta_n}{\delta_n^c} \therefore T_t = \frac{\partial \Phi}{\partial \delta_t} = \left(\frac{\delta_n^c}{\delta_t^c}\right)\frac{\sigma(\lambda)}{\lambda}\frac{\delta_t}{\delta_t^c} \tag{4a, b}$$

where δ_n and δ_t are the normal and tangential components of separation across the interface, and δ_n^c and δ_t^c, their critical terminal values in the pure response modes. The combined separation measure is defined by, λ, as a reasonable mode of response that can be taken as a geometrieal mean of the two pure response modes,

$$\lambda = \sqrt{\left(\frac{\delta_n}{\delta_n^c}\right)^2 + \left(\frac{\delta_t}{\delta_t^c}\right)^2}. \tag{5}$$

Finally, the form of the effective traction response $\sigma(\lambda)$ was taken to be, (Needleman, 1987)

$$\sigma(\lambda) = \sigma_{max}\frac{\lambda}{\lambda_o}\left(\frac{1-\lambda}{1-\lambda_o}\right)^{\frac{1}{\lambda_o}-1}, (0 < \lambda_o < 0.5), \tag{6}$$

similar to the well known, so-called universal Binding Energy Relationship of Rose et al (1984), where σ_{max} is the peak stress and λ_o is the value of λ where the peak stress is reached, and represents the principal shape factor of the (t-s) law while σ_{max} scales its

height. In the present case, of course, the traction separation relation is intended to model the ductile cavitation and dimple fracture across the interface where σ_{max} should represent the interface stress that promotes debonding of the precipitates from the fibers and where the effective range of action of λ respresents a characteristic rupture separation distance of the order of interparticle spacing. Alternatively, the interfacial separation energy, Γ_o and σ_{max} by plastic dimpling can be taken as the two characterizing parameters where,

$$\Gamma_o = \frac{\lambda_o(1-\lambda_o)^{1-\frac{1}{\lambda_o}}}{(1+\lambda_o)}\sigma_{max}\delta_n^c. \tag{7}$$

As a first approximation δ_n^c/δ_t^c was taken as unity and the value of λ_o as 0.3. Parametric studies considered σ_{max} and Γ_o as the two principal scaling factors. These were introduced in normalized form as $(\Gamma_o/\sigma_o b)$ and (σ_{max}/σ_o) in sensitivity studies of the model. For composites with long fibers, $L \gg b, w$, and L_D (the length of debonded interface), the dependence of load should be independent of the cell length L. Indeed, the inelastic separation displacement u^*, defined as,

$$u* = u - \epsilon_{22}^{\infty} L \tag{8}$$

is independent of L, where ϵ_{22}^{∞} is the longitudinal strain at the end, with u being the imposed total axial displacement. Therefore, the dependence of axial load P on imposed inelastic displacement can be written as,

$$\frac{P}{\sigma_0 b} = \mathrm{f}\Big(\frac{u^*}{\epsilon_0 b}; v_f; \frac{\sigma_0}{E}, N, \nu; \frac{E_f}{E}, \nu_f; \frac{\Gamma_0}{\sigma_0 b}, \frac{\sigma_{max}}{\sigma_0}, \frac{\delta_n^c}{\delta_t^c}, \lambda_0\Big), \tag{9}$$

together with parameters of geometry, materials and interface. During the progressive failure of the composite, the work done by the applied load is dissipated in the plastic flow of the matrix strips and in the surface creation due to interfacial decohesion, except the component stored in the material as elastic strain energy. Putting this into the equation, gives

$$\int_0^u P du = \int_V \int_0^{\epsilon^p} \sigma : d\epsilon^p \, dV + \Gamma_0 L_D(u^*) + U^e, \tag{10}$$

where L_D is the length of debonded interface. Both the work input and elastic strain energy U^e depend on the cell length L. However, their difference

$$U^* = \int_0^u P du - U^e = U^p + U^s \tag{11}$$

is independent of L, representing the total irreversible energy dissipation through matrix plastic flow and interfacial debonding. This energy dissipation can be expressed as a function of applied displacement, with geometry, material and interface parameters, as,

$$\frac{U^*}{\sigma_0 \epsilon_0 b^2} = \mathrm{g}\Big(\frac{u^*}{\epsilon_0 b}; v_f; \frac{\sigma_0}{E}, N, \nu; \frac{E_f}{E}, \nu_f; \frac{\Gamma_0}{\sigma_0 b}, \frac{\sigma_{max}}{\sigma_0}, \frac{\delta_n^c}{\delta_t^c}, \lambda_0\Big). \tag{12}$$

For parametric studies, the effects of interface and matrix properties on composite strength, ductility and energy dissipation have been investigated, fixing the parameters of secondary importance. The most significant parameters are the bond strength, interfacial separation energy and matrix hardening. The values of other parameters for typical Al_2O_3 fiber and Al alloy matrix were taken as,

$$v_f = w/(w+b) = 0.5, \quad \nu = \nu_f = 0.3, \quad \frac{\sigma_0}{E} = 1.5 \times 10^{-3}, \quad \frac{E_f}{E} = 6.$$

With the fixed parameters, the load-displacement (9) and energy dissipation (work of fracture) (12) relations can be simplified as

$$\frac{P}{\sigma_0 b} = \mathrm{f}\Big(\frac{u^*}{\epsilon_0 b}; N; \frac{\Gamma_0}{\sigma_0 b}, \frac{\sigma_{max}}{\sigma_0}\Big) \tag{13}$$

$$\frac{U^*}{\sigma_0 \epsilon_0 b^2} = \mathrm{g}\Big(\frac{u^*}{\epsilon_0 b}; N; \frac{\Gamma_0}{\sigma_0 b}, \frac{\sigma_{max}}{\sigma_0}\Big). \tag{14}$$

Main Findings

Figure 5 shows a series of deformed configurations with increasing inelastic tensile displacement for a realistic case of a $10\mu m$ diameter fibers which can be taken as a characteristic normalization length. Contours of effective plastic strain are displayed in every configuration. The plastic deformation originates in the matrix at the corner of the broken fiber due

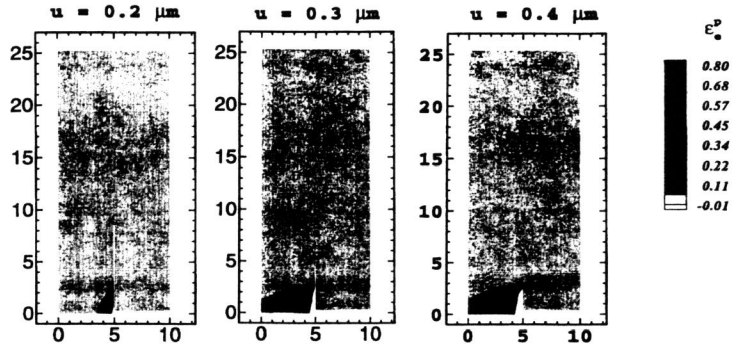

Fig. 5. Deformed configurations of the matrix at a fiber break, for three different levels of axial displacement. Shading shows different levels of effective plastic strain.

to the strain concentration. As the load increases to the peak load, some debonding begins at the fiber/matrix interface governed by the t-s law. Following the load decrease, past the peak load, more and more debonding occurs as the imposed displacement increases further (see figures for $u*$ = 0.2, 0.3, 0.4 μm). This process, accompanied with significant load decrease, is controlled by the fiber/matrix debonding through plastic cavitation.

Following further increases of the imposed displacement, the interface debonding gradually slows down as the traction on the lateral fiber surfaces decreases. The axial load on the fiber is gradually transfered to the matrix and the plastic strains build up in the matrix strip between the corners of two adjacent broken fibers. This causes necking of the the matrix strip, providing ductility to the composite. This process, dominated by matrix necking, has a slower load decrease than the regime by controlled debonding, due to load shedding to the matrix. The distinctive stages, controlled by interface debonding, followed by one dominated by necking, are illustrated clearly in the load-displacement and energy dissipation curves of Figs. 6a-6c.

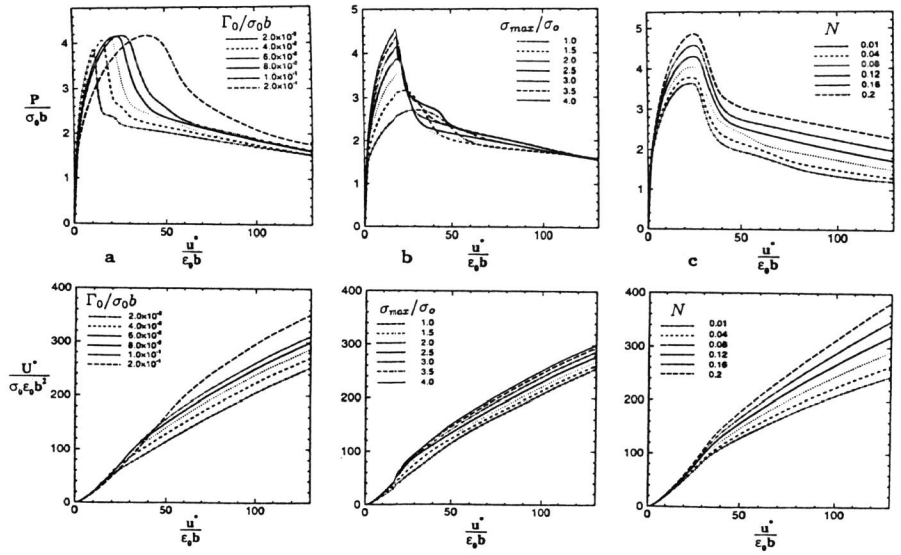

Fig. 6. Load displacement and associated overall energy dissipation curves as a function of normalized inelastic axial displacement: a) effect of debonding energy Γ_o on behavior, for $\sigma_{max}/\sigma_o = 3$ and $N = 0.1$; b) effect of peak stress σ_{max} on behavior, for $\{Gamma_o/\sigma_o b = 6x10^{-2}$ and $N = 0.1$; c) effect of hardening exponent N on behavior for $\Gamma_o/\sigma_o b = 6x10^{-2}$ and $\sigma_{max}/\sigma_o = 3$.

Figure 6 displays the effect of interfacial separation energy Γ_0 on the load-displacement curves and the energy dissipation during the progression of failure for $\sigma_{max}/\sigma_0 = 3$ and $N = 0.1$. The peak load remains roughly at a constant level for various Γ_0's. Actually, the peak load is chiefly determined by the interfacial bond strength between precipitates and fiber, for a matrix with low hardening. The energy dissipation (fracture energy) increases with increasing Γ_0, because more work is required to separate the fiber/matrix interface.

Curves of load-displacement and energy dissipation are shown in Figure 6b for various normalized bond strengths σ_{max}/σ_o (with $\Gamma_0/\sigma_0 b = 6.0 \times 10^{-2}$ and $N = 0.1$). The peak load increases with the interfacial bond strength. High axial composite strength can be achieved with high bond strength at fiber/matrix interface. However, the bond strength has comparatively little effect on the energy dissipation. The small increase in the energy dissipation comes from slight increases of the plastic strains in the matrix.

The most significant factor for the toughness of the composite is matrix strain hardening. Figure 6c displays the load-displacement curves and energy dissipations for various hardening exponents N with fixed interfacial property ($\Gamma_0/\sigma_0 b = 9.0 \times 10^{-2}$ and $\sigma_{max}/\sigma_0 = 3$). Both matrix hardening and interfacial bond strength contribute to the axial strength of the composite. The increases in peak load with matrix hardening is shown in the figure. The fracture energy increases significantly with the hardening exponent. This is due to the larger plastic dissipation in the matrix and a little more debonding along the interface. In contrast to the interfacial bond strength and separation energy, the matrix hardening can provide both higher peak load and larger energy dissipation.

The model for Mode A behavior has confirmed that the fiber/matrix interface plays a very important role in the toughness of the composite system. If the interface strength is low, Γ_o as defined in Eqn (7) will be very low. Interfacial cracks will propagate long distances upon fiber fracture, decoupling the matrix from the fiber. Matrix ligaments will still neck and rupture resulting in acceptable levels of axial work of fracture, but the transverse strength of the composite will be wholly compromised. This appears to be what happens for aging periods less than 100 hrs at 350C in Fig. 2. In the other extreme case, an excessively well bonded fiber/matrix interface will assure a high transverse strength but will minimize the development of matrix strip rupture by promoting premature dilatant plastic behavior and ductile dimpled fracture from matrix particles (type "2" behavior shown in Fig. 1a). This appears to be what happens for aging periods much above 100 hrs at 350C, resulting in significantly reduced work of fracture in the longitudinal direction due to inadequate extent of debonding. Only concurrent interface debonding, accompanying the neck formation and rupture of matrix ligaments will maximize the work of fracture in the Mode A process.

DISCUSSION

The specific metal matrix system of Al_20_3 fibers and the Type 224 casting alloy with its Al_2Cu precipitates respresents the most attractive system that has been experimentally investigated. Other systems with matrixes of *Al-Cu-Mg* and *Al-Mg-Zn* compositions were found to be not as easily controllable leading to either execessive debonding or adhesion so strong as to split the Al_20_3 fibers instead of accomplishing debonding at the interfaces.

We note, moreover, that if the axial tensile strength of the composite σ_{ca} is considered to be a result of the usual rule of mixtures given by,

$$\sigma_{ca} = \nu_f \overline{\sigma}_f^* + (1 - \nu_f)\sigma_m^* \tag{15}$$

(where $\overline{\sigma}_f^*$ is the average fiber tensile strength and σ_m^* the tensile plastic resistance of the matrix at the strain of fiber fractures), and the transverse tensile strength σ_{ct} is governed by an interface flaw of half length a and interface fracture toughness K_c by the relation,

$$\sigma_{ct} = K_c/\sqrt{\pi a}, \tag{16}$$

then the findings represented in Fig. 2 are not fully consistent.

First, peak aging in the matrix is known to raise the plastic resistance of the as-cast material by roughly 65%. At 50% dilution in the composite this should result in an improvement of axial tensile strength by the rule of mixtures of Eqn.(15) by only 33%, or up to 575 MPa while the observed improvement is 125%. Since the actual axial composite stength of 975 MPa is close to being consistent with a rule of mixtures of fiber strength (with a typical reduction in fiber strength due to processing) and peak matrix plastic resistance, we must conclude that the as-cast composites had been damaged in an unspecified manner. The decline of axial composite stength from the peak value of 975 to the level of roughly 770 MPa is also broadley consistent with expectations, reinforcing the view that the as cast composites were damaged.

In the transverse direction between 30 and 100 hrs of aging at 350C the strength increases by a factor of roughly 8. If this were a result only of increasing interface fracture toughness K_c due to particle coarsening by a factor of 2.5, the conventional expectations based on the dependence of K_c on the microstructural scale of interpore (or interparticle) dimensions should have resulted in an improvement of only about 60%. Thus, we must conclude that the dramatic increase in transverse strength must have in large part been due to healing of pre-existing interface flaws by a diffusive process that is quite likely at 350C.

The micromechanical model represents only an initial attempt in linking the experimental observations on fracture governed by interface debonding to a mechanistic framework. It has introduced special methodology capable of dealing with the complex problem of deformation induced mix of modes of interface seperation through a flexible tension/shear, traction/separation relation that can readily admit actual experimental measurements related to such separation, by a proper choice of parameters. In the ranges of parameters presently investigated the model has not demonstrated the reduction of the axial work of fracture X_A $(U^*/\nu_f b)^2$ in the model) of Eqn.(1) due to reduction in debond length L_D. Such reductions will apparently occur with more substantial increases in σ_{max} and λ_o of the traction separaton law of Eqn.(6).

We view the present results with considerable satisfaction and envision a better linkage between the experimental manipulation of the interface microstructure and the micromechanical model.

Acknowledgement

The early experimental research at MIT was supported by the ONR through Contract N00014-85-K-0645. The research on the micromechanical model performed at Brown University was supported by ONR under Grant N00014-95-1-0399.

References

1. Argon, A.S. (1974) in *Composite Materials: Fracture and Fatigue* (L.J. Broutman, ed.), Vol. 5, Chap. 4, pp. 153-190. Academic Press, New York.

2. Friler, J.B., A.S. Argon, and J.A. Cornie, (1993), Strength and Toughness of Carbon Fiber Reinforced Aluminum Matrix Composites. *Mater. Sci. Engng.*, **A162**, 143-152.

3. Needleman, A., (1987), A Continuum Model for Void Nucleation and Inclusion Debonding. *J. Appl. Mech.*, **54**, 523-531.

4. Rose, J.H., J.R. Smith, F. Guinea, and J. Ferrante, (1984), Universal Features of the Equation of State of Metals. *Phys. Rev.*, **B29**, 2963-2969.

5. Seleznev, M.L., J.A. Cornie, and F.A. Armantis Jr., (1993), Improving Mechanical Properties of Nextel 610 Reinforced Al-224 Alloy Through θ Phase Precipitation at Fiber/Matrix Interface: Kinetics fo the Precipitation Process. *J. Mater. Engng. Perform.* **2**, 347-352.

6. Suo, Z., and C.F. Shih, (1993), in *Metal Matrix Composites*, (S. Suresh et al eds.) Chap. 12, pp. 217-232. Butterworth-Heineman.

7. Tvergaard, V., and J.W. Hutchinson, (1993). The Influence of Plasticity on Mixed-Mode Interface Toughness. *J. Mech. Phys. Solids*, **41**, 1119-1135.

8. Varias, A.G., N.P. O'Dowd, R.J. Asaro, and C.F. Shih, (1990). Failure of Bimaterial Interfaces. *Mater. Sci. Engng.*, **A126**, 65-93.